IEEE Access
Multidisciplinary | Rapid Review | Open Access Journal

Received December 26, 2020, accepted January 19, 2021, date of publication January 21, 2021, date of current version February 2, 2021.

Digital Object Identifier 10.1109/ACCESS.2021.3053428

An Original Educational Algorithm Assessing the Behaviours of Angular Frequency Deviations of a Multimachine System in Small Signal Analysis

ROBERTO BENATO[1], (Senior Member, IEEE), NUNZIA CROCAMO[2], GIOVANNI GARDAN[1], (Member, IEEE), GIORGIO M. GIANNUZZI[2], COSIMO PISANI[2], FRANCESCO SANNITI[1], (Member, IEEE), AND ROBERTO ZAOTTINI[2]

[1]Department of Industrial Engineering, University of Padova, 35131 Padua, Italy
[2]TERNA S.p.A., 00156 Rome, Italy

Corresponding author: Roberto Benato (roberto.benato@unipd.it)

This work was supported by the TERNA under Grant ENSIEL/ST 191.

ABSTRACT The paper presents a fully self-implementable algorithm that has demonstrated to be an effective tool for power education at the University of Padova-Department of Industrial Engineering. It deals with the small signal analysis of the electromechanical transients of a multimachine system. The algorithm allows analytically building both the state matrix and the input matrix. Moreover, by exploiting the matrix exponential, the angular frequency deviations of synchronous generators can be computed and plotted so to help students to evaluate transient stability. Besides the full exposition of the algorithm, the paper presents a comparison between a self-implemented linearized dynamic in Matlab environment and the dynamic simulation obtained by the commercial software DIgSILENT PowerFactory.

INDEX TERMS Electromechanical transient, linearized dynamic, power system dynamic, small signal stability.

NOMENCLATURE

Symbol	Quantity	Units
$\mathfrak{A}$	State matrix	-
$\mathbf{A}$	Synchronizing matrix	-
$\boldsymbol{A}_{*i}$	Columns of $\mathbf{A}_{grid}$	-
$A_{\mathrm{mm}}, A_{\mathrm{mr}}, A_{\mathrm{rm}}, A_{\mathrm{rr}}$	Self and mutual terms of $\mathbf{A_{grid}}$	-
$\mathbf{A}_{grid}$	Synchronizing matrix of power flow grid	-
$\mathbf{A}_{gen}$	Synchronizing matrix of generators	-
α_λ	Load dependence by frequency	p.u.
$\mathfrak{B}$	Input matrix	-
c	Fictitious line capacitance p.u.l.	nF/km
$cos\varphi$	Generator power factor	-
$\mathbf{D}$	Damping matrix	-
d	Damping coefficients	-
δ_1, δ_2	Voltage arguments of 1 and 2 nodes	rad
$\delta_1^{\oplus}, \delta_2^{\oplus}, \delta_r^{\oplus}, \delta_m^{\oplus}, \delta_n^{\oplus}$	Voltage phasor arguments of *1, 2, r, m, n* nodes in steady-state regime	rad
d_d	Direct-axis damping coefficients	-
$\Delta\delta(\mathbf{s})$	Voltage phasor angle deviation in L-domain	rad
$\Delta\delta_{\mathbf{G}}$	Independent state variable of the internal generator angle deviations	rad
$\Delta\delta_{\mathbf{G}}^{'}$	Independent state variable of the external generator angle deviations	rad
$\Delta\delta_i(t)$	Small argument increment of *i*-th node	rad
$\Delta\delta_{\mathbf{L}}$	Independent state variable of the load angle deviations	rad

The associate editor coordinating the review of this manuscript and approving it for publication was Lei Chen.

$\Delta\delta_{\mathbf{N}}$	Dependent state variable of the neutral node angle deviations	rad
$\Delta\delta_r(t)$, $\Delta\delta_m(t)$	Argument increment on r and m nodes	rad
ΔP	Active power disturbance	MW
$\mathbf{\Delta p(s)}$	Nodal active power deviation in L-domain	p.u.
$\mathbf{\Delta p_{acc}(s)}$	Accelerating power deviation in L-domain	p.u.
$\mathbf{\Delta p_D(s)}$	Damping active power deviation in L-domain	p.u.
$\mathbf{\Delta p_i(s)}$	Generator active power input deviation in L-domain	p.u.
$\mathbf{\Delta p''_{iG}}$	Independent state variable of mechanical power due to the speed governor action	p.u.
$\mathbf{\Delta p_{iG}(s)}$	Column vector of the i-th generator mechanical power due to the speed governor action	p.u.
d_q	Quadrature-axis damping coefficients	-
$\Delta\omega\mathbf{(s)}$	Angular frequency deviation in L-domain	rad/s
$\Delta\omega_{\mathbf{G}}$	Independent state variable of the internal generator angular frequency deviation	rad/s
$\Delta\omega'_{\mathbf{G}}$	Dependent state variable of the external generator angular frequency deviation	rad/s
$\Delta\omega_{\mathbf{L}}$	Independent state variable of the load angular frequency deviation	rad/s
$\Delta\omega_{\max}$	Maximum value of angular frequency deviation transient	rad/s
$\Delta\omega_{\mathrm{reg}}$	Angular frequency deviation in steady-state regime (after a disturbance)	rad/s
$\Delta\omega_i(t)$	Small frequency increment on i-th node	rad/s
$\Delta\omega_r(t)$, $\Delta\omega_m(t)$	Frequency increment on r and m nodes	rad/s
G	Number of generator nodes	-
g	Regulating energy	p.u.
G'	Number of generator internal nodes	-
H(s)	Regulation transfer function matrix in L-domain	-
$\mathbf{H_G(s)}$	Generator regulation transfer function matrix in L-domain	-
$\mathbf{H'_G, H''_G, T^{-1}}$	Utility diagonal matrices	-
h_{iG}	The i-th diagonal component of $\mathbf{H_G(s)}$	-
$\mathbf{H_L}$	Load dynamic frequency response matrix	-
$\mathbf{H'_L}$	Utility diagonal matrix	-
$\underline{i}^{\oplus}$	Vector of current phasors in steady state	p.u.
$\underline{\mathrm{i}}_{\mathrm{d}}$	Current phasor of the 2-port element collapsed into 1-port element.	p.u.
$\underline{i}^{\oplus}_{\Delta_i}$	Vector of current phasors with argument perturbation on i-th node	p.u.
$\underline{\mathrm{i}}_{\mathrm{m}}$, $\underline{\mathrm{i}}_{\mathrm{r}}$	Current phasors feeding m and r ports	p.u.
ϑ	Intermediate parameter for the calculation of $\mathrm{t}_{\Delta\omega max}$	red
ϑ_{12}	$= \delta_1$, - δ_2	rad
K_R	Regulating energy	MW/Hz
L	Number of load nodes	-
λ	The diagonal component of $\mathbf{H_L}$	-
l	Fictitious line inductance p.u.l.	mH/km
LDPD	**L**inearized **D**ynamic algorithm presented in this paper by the University of **P**a**D**ova	
M	Inertia matrix	-
m	Intermediate parameter for the calculation of $\Delta\omega_{\max}$	-
$\mathbf{M_G}$	Generator inertia matrix	-
MGTP	Malta substation	-
m_{iG}	The i-th diagonal component of $\mathbf{M_G}$	-
$\mathbf{M_L}$	Load dynamic behaviour matrix	-
m_λ	Coefficients of $\mathbf{M_L}$	-
N	Number of other nodes	-
$\underline{\mathrm{n}}_{\mathrm{d}}$	Complex power of the 2-port element collapsed into 1-port element	p.u.
$\underline{n}^{\oplus}_{\Delta_i}$	Vector of complex power with argument perturbation on i-th node	p.u.
n_G	Generator complex power	p.u.
$\underline{\mathrm{n}}_{\mathrm{m}}$	Complex power at m port	p.u.
p_1, p_2	Active power transit in 1 and 2 nodes	p.u.
$\mathrm{p}_{\mathrm{cost}}$	Constant component of p_m	p.u.
p_d	Damping power	p.u.
PF	DIgSILENT **P**ower**F**actory software	-
p_g	Generated active power	p.u.
p_λ	Load active power	p.u.
p_m	Active power at m port	p.u.
P_{Sicily}	Total active power absorbed in Sicily	MW
Q_d	Load share with a dynamic dependence by the frequency	-
$\mathbf{Q_1, Q_2, Q_3}$ $\mathbf{Q_4, Q_5, Q_6}$	Utility sub-matrices	-
Q_s	Load share with a static dependence by the frequency	p.u.

$\boldsymbol{R}$	Exponential matrix	-
r	Fictitious line resistance p.u.l.	Ω/km
σ	Frequency droop	-
S_n	Generator apparent power	MW
T_1, T_R	Main regulation time constants	s
T_{as}	Load stating time	s
t'_d	Direct-axis transient time constant	s
T''_{d0}	Direct-axis sub-transient open-circuit time constant	s
$t_{\Delta\omega max}$	Time instant when maximum value of angular frequency deviation transient occurs	s
T_{ia}	The i-th Turbine+generator starting time	s
TH	**TH**eoretical calculations	
TSO	**T**ransmission **S**ystem **O**perator	
t'_q	Quadrature-axis transient time constant	s
T''_{q0}	Quadrature-axis sub-transient open-circuit time constant	s
$\boldsymbol{u(s)}$	Column vector of the power disturbances	p.u.
v'_1	Voltage behind transient reactance	p.u.
v_1, v_2	Voltage magnitude of internal and external generator nodes	p.u.
$v_1^{\oplus}$, $v_2^{\oplus}$, $v_n^{\oplus}$	Components of vector $\boldsymbol{v}^{\oplus}$	p.u.
$\boldsymbol{v}^{\oplus}$	Vector of node voltage phasors in steady state	p.u.
$\underline{\boldsymbol{v}}^{\oplus}$	Vector of voltage phasors in steady state	p.u.
$\underline{v}_d$	Voltage phasor of the 2-port element collapsed into 1-port element	p.u.
$\underline{\boldsymbol{v}}_{\Delta i}^{\oplus}$	Vector of voltage phasors with argument perturbation on i-th node	p.u.
$\underline{v}_m$, $\underline{v}_r$	Voltage phasors of m and r ports	p.u.
ω_0	Characteristic pulse	rad/s
ω_n	Nominal rated angular frequency	rad/s
x	Direct-axis synchronous reactance	p.u.
$\boldsymbol{x}$	Column vector of the independent state variables	-
ξ	Damping factor	-
ξ_{as}	Load asynchronous portion	p.u.
$x(t)$	Time domain state equation solution	-
$\boldsymbol{x_1}$	Column vector of the dependent state variables	-
x_d	Direct-axis synchronous reactance	p.u.
x'_d	Direct-axis transient reactance	p.u.
x''_d	Direct-axis sub-transient reactance	p.u.
x_q	Quadrature-axis synchronous reactance	p.u.
x'_q	Quadrature-axis transient reactance	p.u.
x''_q	Quadrature-axis sub-transient reactance	p.u.
x_t	Step-up transformer reactance	p.u.
$\underline{\boldsymbol{Y}}$	Admittance matrix	-
$\underline{y}_d$	Shunt admittance of the 2-port element collapsed into 1-port element	p.u.
$\underline{y}_m$, $\underline{y}_r$	Shunt admittances of m and r ports	p.u.
$\underline{z}$	Series impedance between m and r ports	p.u.
φ	Argument of $\underline{z}$	rad
$\omega_N^{\oplus}$	Nominal angular frequency	rad/s
$\omega_r(t)$, $\omega_m(t)$	Angular frequency of r and m nodes	p.u.
$\dot{x}$	Vector of state variables derivatives	-
x	Vector of state variables	-
u	Vector of inputs	-
$\oplus$	Superscript symbol denoting the power flow results	

I. INTRODUCTION

This paper is an enlarged, enriched, and detailed version of [1].

The paper presents the research and education experiences gained, in many years, at the Department of Industrial Engineering of the University of Padova about the electromechanical transients of multimachine systems. The power education inside the Course of Power Systems Analysis has much benefitted from these researches since the students can exploit the didactical effectiveness of the linearized dynamic (or modal or small signal stability analysis) in order to deeply understand which parameters influence the small signal stability the most.

Even if the topic is well covered in technical literature by *monumental* books like J. Machowski [2], R. Marconato [3], E.W. Kimbark [4], P. Kundur [5] and P. Anderson [6], the paper seems to be very useful to the engineers and the students who want to implement the present algorithm for:

- Analytically building the state matrix $\mathfrak{A}$ and the input matrix $\mathfrak{B}$;
- Assessing the angular frequency deviations of the generators in time domain by exploiting the matrix exponential.

In fact, once built the state matrix $\mathfrak{A}$, besides the obvious possibility of computing its eigenvalues and the participation factors, the authors apply the technique to compute and plot the angular frequency deviations in time domain of the involved synchronous generators by means of the matrix exponential. The state matrix approach for the study of power system dynamic behaviour has been introduced by Kundur in [7] and by Castrovilli-Marconato in [8] several years ago. With the introduction of participation factors, the "Selective Modal analysis", presented in [9], overcomes the

ambiguous relationship between modes and state variables of the classical modal analysis. The ''Lyapunov Modal analysis'' proposed in [10], [11] characterizes contributions of the system modes and state variables with their associated integral energy on a finite or infinite time interval.

In the wide field of the modal analysis, the authors develop a self-made matrix-based linearized approach for the study of electromechanical oscillations. This method creates the state matrix starting from Kundur formulations [7] but relying on the principle of active power balance through all nodes of the grid around an operation point. The starting operation point is obtained by the calculation of a power flow, by exploiting another open source code developed by R.B. in [12]. This approach overcomes the classical modal analysis (even if it is always possible to perform it) based on mode shapes, eigenvalues and participation factors [13], and exploits the matrix exponential in order to obtain and visualize the angular frequency deviations of all the generators in time domain. These further investigations allow quickly evaluating the stability of the system without resorting to a deep study of the state matrix $\mathfrak{A}$. Some parts of the algorithm have been already presented by R.B. in [1], [14], [15], but in this paper it is completely generalized and enriched also with a comparison between the angular frequency deviations obtained by the present linearized algorithm and the dynamic simulation obtained by the commercial software PF. This comparison is not performed to necessarily show the agreement between the two methods - which are based on two different mathematical models– but to draw conclusions by means of the results of two methods. The former (PF) solves the whole set of the differential algebraic equations and the latter (LDPD) solves the linear system obtained by the linearization around an operation point.

In order to further validate the results, final behaviours are also compared with the calculations of the theoretical frequency deviations developed in [16]. The main purpose of this paper is to show an original educational state-space approach which uses a unique choice of the state variables based on the active power balance: this approach is useful to better understand the power exchanges – and so the angular frequency deviations – between generators and loads in a multi-machine electrical power system.

At Electrical Engineering of the University of Padova, students implement this algorithm in Matlab environment but other math-packages are possible. The effectiveness of this matrix educational approach is that, at the same time, the students learn about small signal stability analysis, make their own-implementation, transfer power system data and are encouraged to make their own comparisons and considerations. All these skills are fundamental for the engineers of the future power systems. Furthermore, the comparison between self-made linearized Matlab-implemented algorithm and PF can benefit from an interface procedure which has been developed in recent years. Even if it is not the topic of the paper, the paper gives some details of this interface procedure in the Appendix. With regard to the future researches, the authors are attempting to include HVDC links into the algorithm, with the aim of extending the range of its applicability [17]–[21].

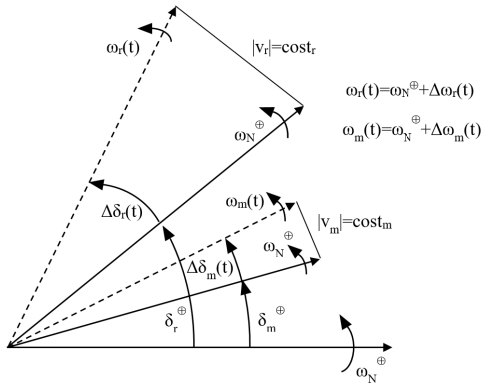

FIGURE 1. Vector representation of voltage phasors for small active power variations (subscripts r and m indicate an internal and an external node of a generator respectively).

II. ANALYTICAL FORMATION OF A AND B MATRIX

The main goal of a linearized dynamic study is to obtain the coefficients of the two matrices namely the state one $\mathfrak{A}$ and input one $\mathfrak{B}$ in (1)

$$\dot{\boldsymbol{x}} = \mathfrak{A}\boldsymbol{x} + \mathfrak{B}\boldsymbol{u} \tag{1}$$

where $\boldsymbol{x}$ is a vector containing the state variables and $\boldsymbol{u}$ is the vector of inputs. In this section, all the formulations useful to analytically build the state matrix $\mathfrak{A}$ and the input matrix $\mathfrak{B}$ are presented. In order to render the presentation more easily explainable, all the matrices shown in the following subsections refer to a benchmark grid (fully presented in section V-A) composed of the following elements:

- 5 internal generator nodes 1÷5: **G** nodes;
- 5 external generator nodes 6÷10: **G'** nodes;
- 8 load nodes 11 ÷ 18: **L** nodes;
- 4 other nodes 19 ÷22: **N** nodes.

Let us assume that the power system to be analysed is in steady-state regime at the initial conditions. The algorithm receives the input states from a single-phase power flow, from which magnitude and argument of the nodal voltage phasors, shown in (2), are obtained:

$$\mathbf{v}^{\oplus} = \begin{bmatrix} v_1^{\oplus} e^{j\delta_1^{\oplus}} \\ v_2^{\oplus} e^{j\delta_2^{\oplus}} \\ \vdots \\ v_n^{\oplus} e^{j\delta_n^{\oplus}} \end{bmatrix} \tag{2}$$

where the superscript symbol $\oplus$ indicates the known steady-state and 1: n are the number of nodes.

Then, active power disturbances of small amplitude are injected into the network nodes. As a consequence, small increments of $\Delta\delta_i(t)$ and $\Delta\omega_i(t)$ are generated, assuming that the voltage magnitudes remain constant at the pre-disturbance value as shown in Fig. 1.

With these assumptions, the behaviour of the dynamic system could be linearized around the operating conditions.

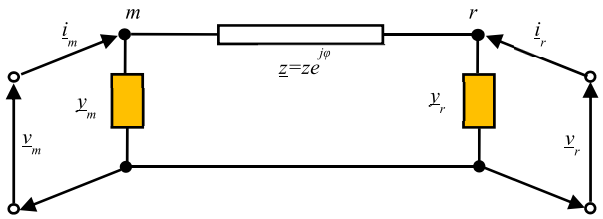

FIGURE 2. Generic 2-port element.

A. THE SYNCHRONISING MATRIX A

The synchronising matrix relates the active power deviations at each node with the voltage phasor angle deviations at each node. The first step is obtaining the synchronising coefficients for a generic 2-port element, then the coefficients for the generator and step-up transformer group are deduced, and finally the total synchronizing matrix is created, by exploiting the primitive and incidence matrices.

It can be proved that if the system is linearised around the steady-state condition, the matrix **A** holds the following properties:

- its elements are constant;
- it is sparse;
- it is singular, i.e. $\det(\mathbf{A}) = 0$;
- it is symmetric.

Let us consider a generic 2-port element placed between two generic ports *m* e *r*, as shown in Fig. 2.

The current feeding the *m*-port can be expressed as:

$$\underline{i}_m = \left(\underline{y}_m + \frac{1}{\underline{z}}\right)\underline{v}_m + \left(-\frac{1}{\underline{z}}\right)\underline{v}_r \tag{3}$$

then the complex power could be calculated as:

$$\underline{n}_m = \underline{v}_m \underline{i}^*_m = \left(\underline{y}^*_m + \frac{1}{z^*}\right)\underline{v}^2_m + \left(-\frac{1}{\underline{z}^*}\right)\underline{v}_m \underline{v}^*_r \tag{4}$$

since the first addendum of (4) is constant with changes in δ_m and δ_r angles, (4) cloud be reformulated as active power:

$$p_m = \mathrm{Re}\left(\underline{n}_m\right) = p_{\mathrm{cost}} - \frac{v_m v_r}{z}\cos\left(\delta_m - \delta_r + \varphi\right) \tag{5}$$

The terms of the synchronizing matrix need the variation of active power entered the *m*-node as a function of δ_m and δ_r angles. In order to obtain that, the partial derivatives around the break-even point should be evaluated as:

$$\begin{cases} \left(\dfrac{\partial p_m}{\partial \delta_m}\right)^{\oplus} = +\dfrac{v^{\oplus}_m v^{\oplus}_r}{z}\sin\left(\delta^{\oplus}_m - \delta^{\oplus}_r + \varphi\right) = \mathrm{A}_{mm} \\ \left(\dfrac{\partial p_m}{\partial \delta_r}\right)^{\oplus} = -\dfrac{v^{\oplus}_m v^{\oplus}_r}{z}\sin\left(\delta^{\oplus}_m - \delta^{\oplus}_r + \varphi\right) = \mathrm{A}_{mr} \\ \left(\dfrac{\partial p_r}{\partial \delta_r}\right)^{\oplus} = +\dfrac{v^{\oplus}_m v^{\oplus}_r}{z}\sin\left(\delta^{\oplus}_m - \delta^{\oplus}_r + \varphi\right) = \mathrm{A}_{rr} \\ \left(\dfrac{\partial p_r}{\partial \delta_m}\right)^{\oplus} = -\dfrac{v^{\oplus}_m v^{\oplus}_r}{z}\sin\left(\delta^{\oplus}_m - \delta^{\oplus}_r + \varphi\right) = \mathrm{A}_{rm} \end{cases} \tag{6}$$

In case of 2-port with only one shunt element, the procedure is similar, and the complex power is obtained by (7).

$$\underline{n}_d = \underline{v}_d \underline{i}^*_d = \underline{v}_d\left(\underline{y}^*_d \underline{v}^*_d\right) = v^2_d \underline{y}^*_d = \underline{n}_{\mathrm{cost}} \tag{7}$$

This means that all the elements that can be represented by a shunt admittance, e.g. loads, do not explicitly contribute to the calculation of the synchronizing coefficients. The most challenging case for **A** coefficient calculation is that of the generators.

A simplified transient model is adopted to represent each synchronous generator and each step-up transformer [2], [24]: this allows simplifying the analysis by neglecting the sub-transient regime. According to this transient model, the generated active power can be expressed as in (8):

$$p_g = \frac{v'_1 v_2}{x'_d + x_t} sin\vartheta_{12} + \frac{v^2_2}{2}\frac{x'_d - x_q}{\left(x'_d + x_t\right)\left(x_q + x_t\right)} sin2\vartheta_{12} \tag{8}$$

considering the two nodes *1* and *2*, where *1* indicates the generator internal fictitious node and *2* indicates the network interface node. Equation (8) is derived with the following assumptions:

- $x_q \equiv x'_q$;
- Absence of active power loss;
- v'_1 is the voltage behind the transient reactance;
- v_2 is the terminal voltage;
- $\vartheta_{12} = \delta_1 - \delta_2$.

The values of v'_1, v_2 and ϑ_{12} are obtained from the preliminary (and always necessary) power flow study of the whole system. Under the assumption of absence of power losses, the relation (9) yields

$$p_2 = -p_1 \tag{9}$$

Consequently, the derivatives of (8) with respect to the angles δ_1 and δ_2 are given by (10) i.e.:

$$\begin{cases} \dfrac{\partial p_1}{\partial \delta_1} = \dfrac{v'_1 v_2}{x'_d + x_t} cos\vartheta_{12} + v^2_2 \dfrac{x'_d - x_q}{\left(x'_d + x_t\right)\left(x_q + x_t\right)} cos2\vartheta_{12} = A_{11} \\ \dfrac{\partial p_1}{\partial \delta_2} = -\dfrac{v'_1 v_2}{x'_d + x_t} cos\vartheta_{12} - v^2_2 \dfrac{x'_d - x_q}{\left(x'_d + x_t\right)\left(x_q + x_t\right)} cos2\vartheta_{12} = A_{12} \\ \dfrac{\partial p_2}{\partial \delta_2} = \dfrac{v'_1 v_2}{x'_d + x_t} cos\vartheta_{12} + v^2_2 \dfrac{x'_d - x_q}{\left(x'_d + x_t\right)\left(x_q + x_t\right)} cos2\vartheta_{12} = A_{22} \\ \dfrac{\partial p_2}{\partial \delta_1} = -\dfrac{v'_1 v_2}{x'_d + x_t} cos\vartheta_{12} - v^2_2 \dfrac{x'_d - x_q}{\left(x'_d + x_t\right)\left(x_q + x_t\right)} cos2\vartheta_{12} = A_{21} \end{cases} \tag{10}$$

It is worth noting that, in this case, the matrix is symmetric since the absence of active power losses into the generator is supposed.

The construction of the final synchronising matrix goes through two different matrices. One named $\mathbf{A}_{\mathrm{grid}}$, whose coefficients are obtained by (6), and one named $\mathbf{A}_{\mathrm{gen}}$ whose coefficients are obtained by (10). The final synchronising matrix **A** is obtained from the sum of the two matrices, as shown in Fig. 3.

A numerical derivation procedure to compute these two matrices is implemented. This numeric procedure exploits vector calculus to automatically compute the coefficients in (6). Starting from the nodal voltage vector in (2), the current and the complex power entering each node is obtained from (11), by exploiting the grid admittance matrix $\underline{\boldsymbol{Y}}$.

$$\begin{aligned} \underline{\boldsymbol{i}}^{\oplus} &= \underline{\boldsymbol{Y}}\,\underline{\boldsymbol{v}}^{\oplus} \\ \underline{\boldsymbol{n}}^{\oplus} &= \underline{\boldsymbol{v}}^{\oplus} \times \underline{\boldsymbol{i}}^{\oplus *} \end{aligned} \tag{11}$$

A numerical increment of $\Delta\delta$ is applied to the argument of the i-th voltage phasor, obtaining (12) i.e.

$$\boldsymbol{v}^{\oplus}_{\Delta i} = \begin{bmatrix} v_1^{\oplus} e^{j\delta_1^{\oplus}} \\ v_2^{\oplus} e^{j\delta_2^{\oplus}} \\ \vdots \\ v_i^{\oplus} e^{j(\delta_i^{\oplus}+\Delta\delta)} \\ \vdots \\ v_n^{\oplus} e^{j\delta_n^{\oplus}} \end{bmatrix} \tag{12}$$

Then the current and the apparent power are calculated again with (13):

$$\begin{aligned} \underline{\boldsymbol{i}}^{\oplus}_{\Delta \mathrm{i}} &= \underline{\boldsymbol{Y}}\,\underline{\boldsymbol{v}}^{\oplus}_{\Delta i} \\ \underline{\boldsymbol{n}}^{\oplus}_{\Delta i} &= \underline{\boldsymbol{v}}^{\oplus}_{\Delta i} \times \underline{\boldsymbol{i}}^{\oplus *}_{\Delta i} \end{aligned} \tag{13}$$

Eq. (14) finally calculates the first column of the matrix.

$$\mathrm{Re}\left(\frac{\underline{\boldsymbol{n}}_{\Delta i} - \underline{\boldsymbol{n}}^{\oplus}}{\Delta\delta}\right) = \begin{bmatrix} \dfrac{\partial p_1}{\partial \delta_i} \\ \vdots \\ \dfrac{\partial p_i}{\partial \delta_i} \\ \vdots \\ \dfrac{\partial p_n}{\partial \delta_i} \end{bmatrix} = \boldsymbol{A}_{*i} \tag{14}$$

Similarly, the other columns are computed by applying the voltage phasor argument increment to the remaining nodes.

The complete matrix **A** in Fig. 4 is obtained by applying the superposition principle. It relates the nodal active power deviations to the voltage phasor angle deviation following (15).

$$\Delta\mathbf{p}(s) = \mathbf{A}\Delta\boldsymbol{\delta}(\mathbf{s}) = \mathbf{A}\frac{\Delta\boldsymbol{\omega}(s)}{s} \tag{15}$$

The matrix **A** is always singular since any sum of row-elements is null [4], [25].

B. DAMPING MATRIX D

The damping matrix ***D*** accounts for the presence of damping windings in synchronous generators. It holds the damping coefficients d, as shown in Fig. 5.

These elements d are computed by using the procedure described by Kimbark [5], derived from Dahl [26] and Park, and by expressing in network p.u. the generator parameters. These coefficients are related to the presence of damping windings, which act during the electromechanical transient

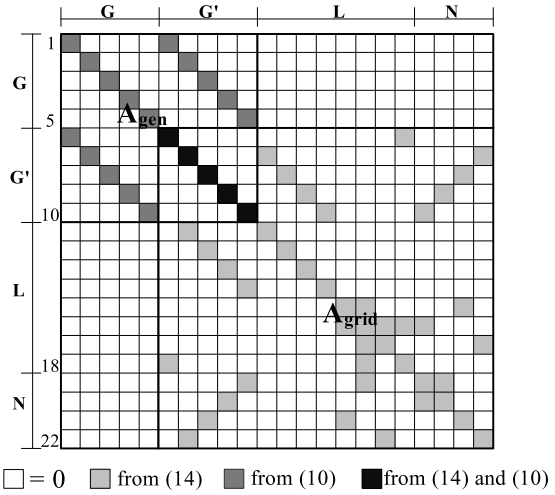

FIGURE 3. Matrix A of the synchronising coefficients obtained from the blending of the two matrices $\mathbf{A_{grid}}$ and $\mathbf{A_{gen}}$.

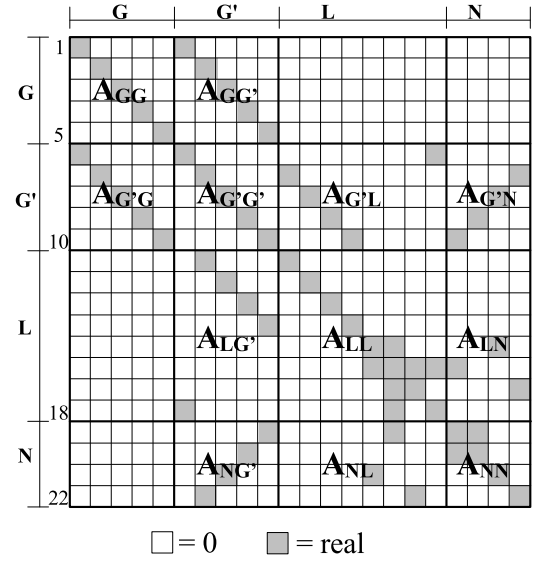

FIGURE 4. Matrix A of the synchronising coefficients.

and change the power output as a function of the magnetic flux variation according to (16):

$$p_d = v_2^2\left[d_d \sin^2\delta + d_q \cos^2\delta\right]\cdot\Delta\omega = v_2^2 \cdot d \cdot \Delta\omega \tag{16}$$

where coefficients d_d and d_q are equal to:

$$\begin{aligned} d_d &= \frac{\left(x'_d - x''_d\right)T''_{d0}}{\left(x + x'_d\right)^2} \\ d_q &= \frac{\left(x'_q - x''_q\right)T''_{q0}}{\left(x + x'_q\right)^2} \end{aligned} \tag{17}$$

Moreover, since an infinite power network is considered, the x term could be assumed equal to zero so that (17) can be

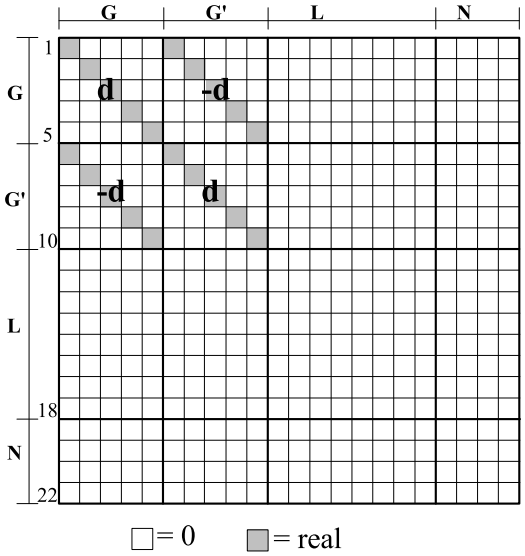

FIGURE 5. Matrix D of the damping coefficients.

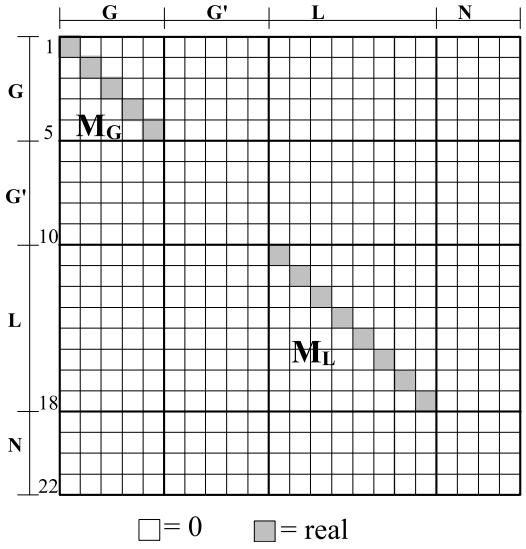

FIGURE 6. Matrix M of the inertia coefficients.

rewritten as:

$$d_d = \frac{x'_d - x''_d}{\left(x'_d\right)^2} T''_{d0}$$
$$d_q = \frac{x'_q - x''_q}{\left(x'_q\right)^2} T''_{q0} \tag{18}$$

Finally, these coefficients allow building the **D** matrix, already shown in Fig. 2, which relates the power output variations due to the damping windings to the angular frequency deviations, as in the following:

$$\Delta \mathbf{p_D}(s) = \mathbf{D} \Delta \boldsymbol{\omega}(s) \tag{19}$$

C. TURBINE + GENERATOR INERTIA COEFFICIENT MATRIX M

The matrix **M** is composed of 2 different matrices: one related to the generator inertia ($\mathbf{M_G}$), and the other one related to the load dynamic behaviour ($\mathbf{M_L}$). Each term of the diagonal matrix $\mathbf{M_G}$ is expressed as:

$$m_{iG} = \frac{n_G \cdot \cos\varphi \cdot T_{ia}}{\omega_n} \tag{20}$$

with T_{ia} [s] = *i-th* Turbine + Generator group starting time. In order to compute both the state and the input matrices, the model must be updated to consider also the load dynamic behaviour: a sub-matrix $\mathbf{M_L}$ accounts for load inertia coefficients and a sub-matrix $\mathbf{H_L}$ for dynamic load behaviour (Fig. 6). Each term of the diagonal matrix $\mathbf{M_L}$ is expressed as in (21):

$$m_\ell = \frac{p_\ell \cdot \xi_{as} \cdot T_{as}}{\omega_n} \tag{21}$$

with ξ_{as} the load asynchronous portion (e.g. $0.8 \div 0.9$) and T_{as} the starting time (e.g. $2 \div 3$ [s]).

Eventually, the matrix in Fig. 6 is obtained: it relates the accelerating power $\mathbf{p_{acc}}$ to the derivative of the angular frequency deviation as in (22):

$$\Delta \mathbf{p_{acc}}(s) = \mathrm{M} \cdot s \Delta \boldsymbol{\omega}(s) \tag{22}$$

D. PRIME MOVER + SPEED REGULATION TRANSFER FUNCTION MATRIX H(S)

The matrix **H** is composed of two different matrices: the former is related to the generator regulation and prime mover ($\mathbf{H_G}$), and the latter is related to the load dynamic frequency response ($\mathbf{H_L}$). Each term of the diagonal matrix $\mathbf{H_G}(s)$ is expressed as in (23):

$$h_{iG} = -g \frac{1 + sT_1}{1 + sT_R} \cdot P(s) \tag{23}$$

where T_1 and T_R are the main regulation constants of the speed governor [22], $P(s)$ is the prime mover transfer function obtained e.g. by [23], $g = \frac{n_G \cdot cos\varphi}{\sigma \omega_n}$, being $n_G\ cos\varphi$ the nominal active power [p.u.] of the *i-th* generator, σ [p.u.] the corresponding speed governor droop, ω_n [rad/s] the rated angular frequency. In this paper, the authors assume the contribution of the prime mover function as a unity gain, in order to provide for a clearer formulation. They consider didactically meaningful to let the students modify the prime mover transfer function in order to understand the displacement introduced by the turbine delay. The elements of the diagonal matrix $\mathbf{H_L}$ are:

$$\ell = \frac{\alpha_\ell p_\ell}{\omega_n} \tag{24}$$

where the parameter α_ℓ characterises the dependence of load upon $\Delta\omega_\ell$ and can range from 2 to -0.5; p_ℓ is the steady-state active load power in [p.u.] and ω_n is the nominal (rated) angular frequency. The final expression of the correlation

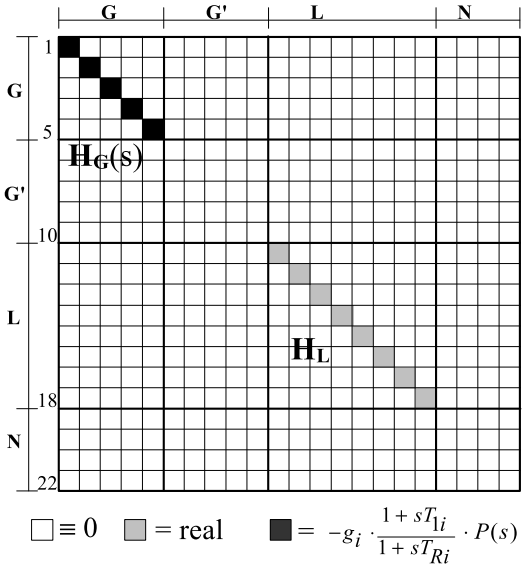

FIGURE 7. Matrix H of the speed regulation coefficients.

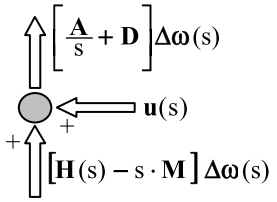

FIGURE 8. Power [p.u.] balance.

between the generator power input and the frequency deviation is expressed by (25). The final matrix is shown in Fig. 7.

$$\Delta\mathbf{p_i}(s) = \mathbf{H}(s) \cdot \Delta\boldsymbol{\omega}(s) \tag{25}$$

E. FINAL SETTLEMENT OF THE STATE MATRIX A AND INPUT MATRIX

The power variations can be represented by means of the power balance scheme shown in Fig. 8.

In Fig. 8, $\mathbf{u}(s)$ [p.u.] is the column vector of the power disturbances injected into each node. The power balance of Fig. 8 can be written as:

$$\left[\frac{\mathbf{A}}{\mathrm{s}} + \mathbf{D} - \mathbf{H}(\mathrm{s}) + \mathrm{s}\cdot\mathbf{M}\right] \cdot \Delta\boldsymbol{\omega}(\mathrm{s}) = \mathbf{u}(\mathrm{s}) \tag{26}$$

and by matrix inversion:

$$\Delta\boldsymbol{\omega}(\mathrm{s}) = \left[\frac{\mathbf{A}}{\mathrm{s}} + \mathbf{D} - \mathbf{H}(\mathrm{s}) + \mathrm{s}\cdot\mathbf{M}\right]^{-1} \mathbf{u}(\mathrm{s}) \tag{27}$$

The general use of (27) is considerably complex due to the inversion of a matrix, which is function of s; however, its use is easy if the numerical computation of the harmonic response to a disturbance vector $\mathbf{u}\cdot e^{j\omega t}$ is considered: some useful information on the dynamic behaviour of the linearized system can be deduced. Similarly to the procedures in [15], it is worth nothing that the vector of the mechanical power due to the speed governor action in (28):

$$\Delta\mathbf{p_{iG}}(\mathrm{s}) = \mathbf{H_G}(\mathrm{s}) \cdot \Delta\boldsymbol{\omega_G}(\mathrm{s}) \tag{28}$$

can be expressed in the time domain as:

$$\Delta\mathbf{p_{iG}}(\mathbf{t}) = \mathbf{H'_G}\Delta\boldsymbol{\omega_G}(\mathbf{t}) + \Delta\mathbf{p''_{iG}}(\mathbf{t}). \tag{29}$$

For the state variable vector, the following relationship can be written:

$$\Delta\dot{\mathbf{p}}''_{\mathbf{iG}} = \mathbf{H''_G}\Delta\boldsymbol{\omega_G} - \mathbf{T^{-1}}\Delta\mathbf{p''_{iG}} \tag{30}$$

where $\mathbf{H'_G}$, $\mathbf{H''_G}$, $\mathbf{T^{-1}}$ are diagonal matrices with constant terms. Once opportunely partitioned the matrices $\mathbf{A}$, $\mathbf{D}$, $\mathbf{H}(s)$, $\mathbf{M}$, the dynamic power balance in the time domain leads to the expression in (31), as shown at the bottom of the next page.

In (31) it has:

- $\mathbf{x}$ is the column vector of the independent state variables: $\mathbf{x^t} = \Delta\boldsymbol{\delta}^{\mathbf{t}}_{\mathbf{G}}, \Delta\boldsymbol{\delta}^{\mathbf{t}}_{\mathbf{G}'}, \Delta\boldsymbol{\delta}^{\mathbf{t}}_{\mathbf{L}}, \Delta\boldsymbol{\omega}^{\mathbf{t}}_{\mathbf{G}}, \Delta\boldsymbol{\omega}^{\mathbf{t}}_{\mathbf{L}}, \Delta\mathbf{p}''^{\mathbf{t}}_{\mathbf{G}}$;
- $\mathbf{x_1}$ is the column vector of the dependent state variables: $\mathbf{x}^{\mathbf{t}}_{\mathbf{1}} = \Delta\boldsymbol{\omega}^{t}_{G'}, \Delta\boldsymbol{\delta}^{\mathbf{t}}_{\mathbf{N}}$.

The last part of the power balance can be expressed as a function of disturbances, inertia and speed regulation coefficients as in (32):

$$\begin{pmatrix} \Delta\mathbf{p_G} = \mathbf{u_G} + \mathbf{H'_G}\Delta\boldsymbol{\omega_G} + \Delta\mathbf{p''_G} - \mathbf{M_G}\Delta\dot{\boldsymbol{\omega}}_{\mathbf{G}} \\ \Delta\mathbf{p_L} = \mathbf{u_L} + \mathbf{H_L}\Delta\boldsymbol{\omega_L} - \mathbf{M_L}\Delta\dot{\boldsymbol{\omega}}_{\mathbf{G}} \\ \Delta\mathbf{p_{G'}} = \mathbf{u_{G'}} \\ \Delta\mathbf{p_N} = \mathbf{u_N} \end{pmatrix} \tag{32}$$

By comparing (31) with (32), the following new relationships (33) can be obtained, as shown at the bottom of the next page:

The above matrix relation can be rewritten with reference to the new $\mathbf{Q_1} \div \mathbf{Q_6}$ sub-matrices as in (34-36).

$$-\mathbf{M_G}\Delta\dot{\boldsymbol{\omega}}_{\mathbf{G}} = \mathbf{Q_1 x} + \mathbf{Q_2 x_1} - \mathbf{u_G} \tag{34}$$

$$-\mathbf{M_L}\Delta\dot{\boldsymbol{\omega}}_{\mathbf{L}} = \mathbf{Q_3 x} + \mathbf{Q_4 x_1} - \mathbf{u_L} \tag{35}$$

$$\mathbf{0} = \mathbf{Q_5 x} + \mathbf{Q_6 x_1} - \mathbf{u_{G'N}} \tag{36}$$

Equation (36) holds the dependent state vector

$$\mathbf{x_1} = \mathbf{Q_6^{-1}}\mathbf{u_{G'N}} - \mathbf{Q_6^{-1}}\mathbf{Q_5 x} \tag{37}$$

by introducing (37) in (34) and (35), it is possible to obtain the fourth and fifth state equation (38-39).

$$\begin{aligned} \Delta\dot{\boldsymbol{\omega}}_{\mathbf{G}} = & -\mathbf{M_G^{-1}}\left(\mathbf{Q_1} - \mathbf{Q_2}\mathbf{Q_6^{-1}}\mathbf{Q_5}\right)\mathbf{x} \\ & -\mathbf{M_G^{-1}}\mathbf{Q_2}\mathbf{Q_6^{-1}}\mathbf{u_{G'N}} + \mathbf{M_G^{-1}}\mathbf{u_G} \end{aligned} \tag{38}$$

$$\begin{aligned} \Delta\dot{\boldsymbol{\omega}}_{\mathbf{L}} = & -\mathbf{M_L^{-1}}\left(\mathbf{Q_3} - \mathbf{Q_4}\mathbf{Q_6^{-1}}\mathbf{Q_5}\right)\mathbf{x} \\ & -\mathbf{M_L^{-1}}\mathbf{Q_4}\mathbf{Q_6^{-1}}\mathbf{u_{G'N}} + \mathbf{M_L^{-1}}\mathbf{u_L} \end{aligned} \tag{39}$$

The first state equation is the obvious identity written for $\mathbf{G}$ nodes i.e.:

$$\Delta\dot{\boldsymbol{\delta}}_{\mathbf{G}} = \mathbf{I_5}\Delta\boldsymbol{\omega_G} \tag{40}$$

The second state equation may be expressed according to the following equation:

$$\dot{\mathbf{\Delta}}\boldsymbol{\delta}_{\mathbf{G}} = \mathbf{\Delta}\boldsymbol{\omega}_{\mathbf{G}} = \begin{bmatrix} 1 & & & & & & & & \\ & 1 & & & & & & & \\ & & 1 & & & & & & \\ & & & 1 & & & & & \\ & & & & 1 & & & & \end{bmatrix}$$

$$\mathbf{x}_1 = -\mathbf{Q}_7\mathbf{Q}_6^{-1}\mathbf{Q}_5\mathbf{x} + \mathbf{Q}_7\mathbf{Q}_6^{-1}\mathbf{u}_{\mathbf{G'N}} \tag{41}$$

The third state equation is the obvious identity written for L nodes:

$$\mathbf{\Delta}\dot{\boldsymbol{\delta}}_{\mathbf{L}} = \mathbf{I}_8\mathbf{\Delta}\boldsymbol{\omega}_{\mathbf{L}} \tag{42}$$

The sixth state equation is given directly by (30). By assembling the six state equations, the matrix relation (43), as shown at the bottom of the next page, can be written so that the system state matrix $\mathfrak{A}$ and the input matrix $\mathfrak{B}$ are *analytically computed*, as shown at the bottom of the next page.

III. ANGULAR FREQUENCY DEVIATIONS IN TIME DOMAIN

Once the system state matrix $\mathfrak{A}$ and the input matrix $\mathfrak{B}$ are completely computed as described in section II, it is possible to achieve the time domain response of the linearized system following a disturbance $\mathbf{u(t)}$. The time domain response involves the extensive use of the matrix exponential function.

The solution of the state equation $\dot{x} = \mathfrak{A}x + \mathfrak{B}u$ can be expressed in the elegant matrix form by (44).

$$x(t) = e^{\mathfrak{A}\cdot t}x(0) + \int_0^t e^{\mathfrak{A}\cdot(t-\tau)}\mathfrak{B}u(\tau)\,d\tau \tag{44}$$

where $e^{\mathfrak{A}t}$ represents the matrix exponential of the state matrix $\mathfrak{A}$. Several different methods of calculation of $e^{\mathfrak{A}t}$ are given in textbooks, e.g. [27], [28]. However, in many math-packages the matrix exponential is a native function.

The integral in (44) expresses the forced response and its solution involves the inverse of the matrix $\mathfrak{A}$, as follows [29]:

$$\int_0^t e^{\mathfrak{A}\cdot(t-\tau)}\mathfrak{B}u(\tau)\,d\tau = \mathfrak{A}^{-1}e^{t\mathfrak{A}}\mathfrak{B}\mathbf{u(t)}. \tag{45}$$

Since the matrix $\mathfrak{A}$ is singular, the integral could not be computed in such a form.

DeCarlo demonstrates [30] that this kind of integral can be evaluated by using the matrix exponential technique when the input $\mathbf{u}$ on the system is constant so that its derivative is null i.e. $\dot{\mathbf{u}} \equiv \mathbf{0}$.

DeCarlo introduces a new state matrix $\mathbf{R}$ as shown in Fig. 9(a) and indicates that the seeking integral is given simply by $\mathbf{R_{12}u}$ ($\mathbf{u}$ is constant) as shown in Fig. 9(b).

The implementation of these formulations allows plotting the state variable behaviours in time domain, so giving a more direct and clarifying indication on the stability of a multimachine system.

$$\begin{bmatrix} \Delta p_G \\ \Delta p_L \\ \Delta p_{G'} \\ \Delta p_N \end{bmatrix} = \begin{bmatrix} A_{GG} & A_{GG'} & & d & & & -d & \\ & A_{LG'} & A_{LL} & & & & & A_{LL} \\ A_{G'G} & A_{G'G'} & A_{G'L} & -d & & & d & A_{G'N} \\ & A_{NG'} & A_{NL} & & & & & A_{NN} \end{bmatrix} \cdot \begin{bmatrix} \\ x \\ \\ x_1 \end{bmatrix} \tag{31}$$

$$\begin{bmatrix} -M_G\,\Delta\dot{\omega}_G \\ -M_L\,\Delta\dot{\omega}_L \\ 0 \\ 0 \end{bmatrix} \begin{matrix} Q_1 \\ Q_3 \\ = \\ Q_5 \end{matrix} \begin{bmatrix} A_{GG} & A_{GG'} & & d - H'_G & & -I_5 & -d & \\ & A_{LG'} & A_{LL} & & -H'_L & & & A_{LL} \\ A_{G'G} & A_{G'G'} & A_{G'L} & -d & & & d & A_{G'N} \\ & A_{NG'} & A_{NL} & & & & & A_{NN} \end{bmatrix} \begin{matrix} Q_2 \\ Q_4 \\ \cdot \\ Q_6 \end{matrix} \begin{bmatrix} \\ x \\ \\ x_1 \end{bmatrix} - \begin{bmatrix} u_G \\ u_L \\ u_{G'} \\ u_N \end{bmatrix} \quad u_{G'N} \tag{33}$$

$$\mathbf{R} = \begin{bmatrix} \mathfrak{A} & \mathfrak{B} \\ \mathbf{0} & \mathbf{0} \end{bmatrix} \quad \text{(a)}$$

$$e^{\mathbf{R}t} = \begin{bmatrix} \mathbf{R_{11}}(t) & \mathbf{R_{12}}(t) \\ \mathbf{0} & \mathbf{I} \end{bmatrix} = \sum_{k=0}^{\infty} \frac{R^k t^k}{k!} \quad \text{(b)}$$

FIGURE 9. New state matrix and its exponential.

IV. COMPARISON BETWEEN LDPD AND PF ANGULAR FREQUENCY DEVIATION BEHAVIOURS

With the aim of comparing the dynamic behaviour of the linearized system following a disturbance with that of a ''real'' system, three case studies are presented in section V-A, V-B and V-C: they are also compared with PF. In section V-A a 17-bus grid is presented, in section V-B the number of buses is increased to 29 buses with the aim of testing the robustness of the algorithm. Other reference grids have been implemented but they are not reported in this paper. However, a real case seems to be extremely effective to perform a comparison, so in section V-C the Sicily grid is implemented and the small signal analysis is performed on it. Some assumptions are adopted in the PF model to compare the results in a rigorous manner. The generator model implemented in the linearized dynamic is of the type ''constant voltage behind transient reactance'', and the model adopted in PF is the Model 2.2 [31], according to [32]. Since the LDPD generator model does not take into account the sub-transient regime, in some comparisons with PF, it is necessary to ''freeze'' the transient regime into the PF generator model, setting sub-transient reactances (x''_d and x''_q) equal to the transient ones (x'_d and x'_q) and the transitory time constant t'_d and t'_q to a very high value. In addition, the prime mover function is considered as a unity gain also in PF, with the aim of performing comparisons all factors being equal.

A. 17-BUS GRID CASE STUDY

In this section the reference grid introduced in section II is implemented into PF (see Fig. 10). The study of such a simplified network offers the opportunity to compare results with a theoretical evaluation of the angular frequency behaviour, described in [16] and valid for a single generator + loads.

This analytical approach allows computing the angular frequency deviation after the transient (46), its peak value (47), and the time at which the maximum peak occurs (48)

$$\Delta\omega_{reg} = -2\pi \frac{\Delta P}{K_R} \quad (46)$$

$$\Delta\omega_{\max} = -2\pi(1+m)\frac{\Delta P}{K_R} \quad (47)$$

$$t_{\Delta\omega\,\max} = \frac{\vartheta}{\omega_0\sqrt{1-\xi^2}} \quad (48)$$

where K_R is the regulating energy of the entire network, ΔP is the disturbance, ξ is the damping factor, ω_0 is the characteristic pulse and ϑ and m are two intermediate parameters [16]. On this basis, let us compute the grid dynamic after a *10%* step decrease of the load at node *6* (*1* MW of nominal power).

Fig. 11 shows the behaviours of the angular frequency deviation of the slack bus generator (**G1**) computed with the two approaches.

The agreement between LDPD and PF impresses, with a difference less than 2% (see Table 1). It is also interesting to note the behaviours of the angular frequency deviations of the other generators computed with the abovementioned simplifications on the PF generator model (see Fig. 12) and by considering the complete generator model in PF without

$$\begin{bmatrix} \dot{\Delta\delta}_G \\ \dot{\Delta\delta}_{G'} \\ \dot{\Delta\delta}_L \\ \dot{\Delta\omega}_G \\ \dot{\Delta\omega}_L \\ \dot{\Delta p}''_G \end{bmatrix} = \begin{bmatrix} \mathbf{I_5} & & & & & \\ \mathbf{-Q_7\,Q_6^{-1}\,Q_5} & & & & & \\ & \mathbf{I_8} & & & & \\ \mathbf{-M_G^{-1}\,(Q_1 - Q_2\,Q_6^{-1}\,Q_5)} & & & & & \\ \mathbf{-M_L^{-1}\,(Q_3 - Q_2\,Q_6^{-1}\,Q_5)} & & & & & \\ & \mathbf{H''_G} & & \mathbf{T^{-1}} & & \end{bmatrix} \begin{bmatrix} \Delta\delta_G \\ \Delta\delta_{G'} \\ \Delta\delta_L \\ \Delta\omega_G \\ \Delta\omega_L \\ \Delta p''_G \end{bmatrix} + \begin{bmatrix} & & & \\ \mathbf{Q_7\,Q_6^{-1}} & & & \\ & & & \\ \mathbf{M_G^{-1}} & & \mathbf{-M_G^{-1}\,Q_2\,Q_6^{-1}} & \\ & \mathbf{M_L^{-1}} & \mathbf{-M_L^{-1}\,Q_4\,Q_6^{-1}} & \\ & & & \end{bmatrix} \begin{bmatrix} u_G \\ u_L \\ u_{G'} \\ u_N \end{bmatrix} \quad (43)$$

$$\dot{\mathbf{x}} \qquad \mathfrak{A} \qquad \mathbf{x} \qquad \mathfrak{B} \qquad \mathbf{u}$$

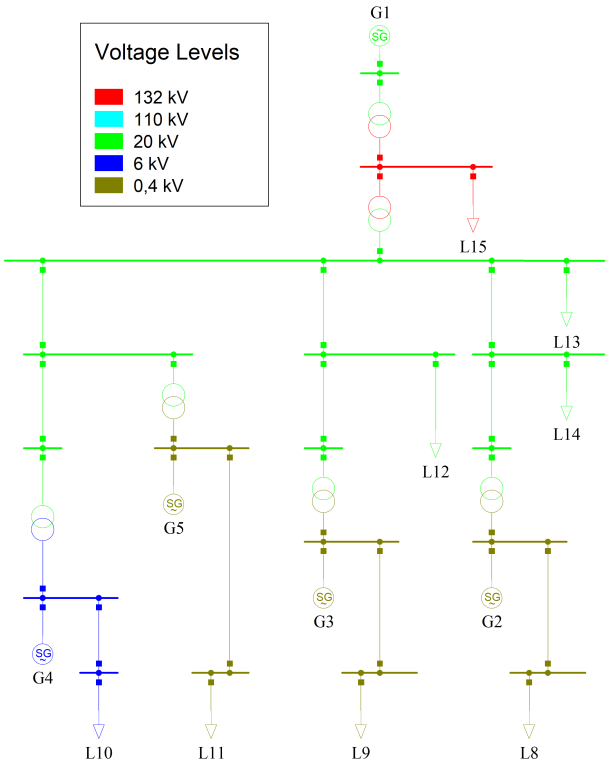

FIGURE 10. Single-line diagram of the analysed power system in PF.

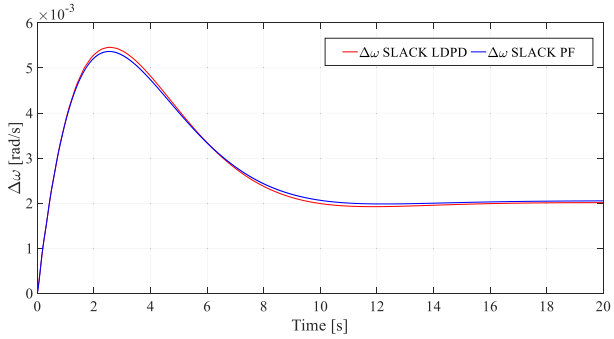

FIGURE 11. Angular frequency deviations of the slack-bus after a disturbance with LDPD and with PF.

"freezing" of transient regime (see Fig. 13). Fig. 13 shows a considerable displacement in the damping contribution between PF and LDPD results. These mismatches are due to the different mathematical model adopted for the LDPD, based on the transient reactance.

This is confirmed by the simulation performed in Fig. 12 by "freezing" the transient regime also in the PF generator model. In fact, the damping factor in this case is the same for the two methods.

It can be seen how the linearized dynamic enhances the oscillatory phenomena (with a less damping effect) with respect to PF using a complete generator model. Nevertheless, it is impressive to note the good agreement between the two dynamics during the first second of the transient, just when the small signal stability is settled.

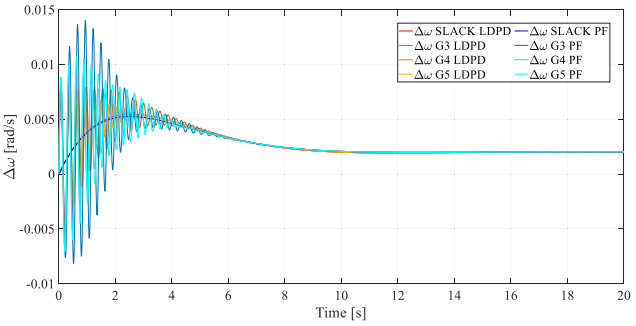

FIGURE 12. Angular frequency deviations of all the generator buses after a disturbance with LDPD and with PF: simplified PF generator model.

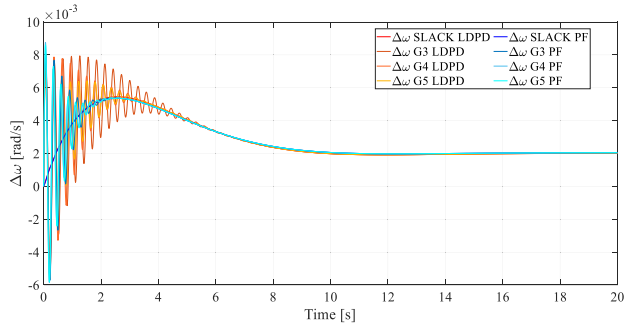

FIGURE 13. Angular frequency deviations of all the generator buses after a disturbance with LDPD and with PF: complete PF generator model.

TABLE 1. Comparison of absolute values and percentage errors of dynamic response quantities.

		Theoretical – One generator plus Loads (TH)	*LDPD*	*PF*
$\Delta\omega_{reg}$	[rad/s]	0.00186	0.00201	0.00205
	%	8 *	-	1.95 **
$\Delta\omega_{max}$	[rad/s]	0.00499	0.00546	0.00537
	%	9.33 *	-	-1.69 **
$\Delta\omega_{reg}$	[rad/s]	2.586	2.56	2.556
	%	-1 *	-	-0.16 **
* Percent difference $\frac{LDPD-TH}{TH}\cdot 100$				
** Percent difference $\frac{PF-LDPD}{LDPD}\cdot 100$				

B. 29-BUS GRID CASE STUDY

In this case study, the number of nodes is increased up to 29 to verify whether LDPD gives good results as network complexity increases. Fig. 14 shows the network implemented in PF.

Let us compute the grid dynamic after a 10% step decrease of the load at node 20 (1 MW of nominal power). Fig. 15 shows the angular frequency deviation behaviour in the slack bus computed with LDPD and with PF.

Once again, the agreement between the dynamic simulation and the linearized one is very good, with a difference less than 4% in the maximum value of the angular frequency deviation (see Table 2). Fig. 15 also shows the angular fre-

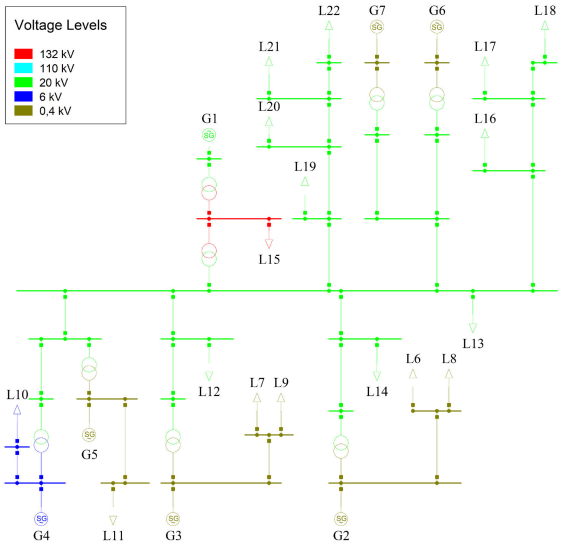

FIGURE 14. Single-line diagram of the 29-bus analysed power system in PF.

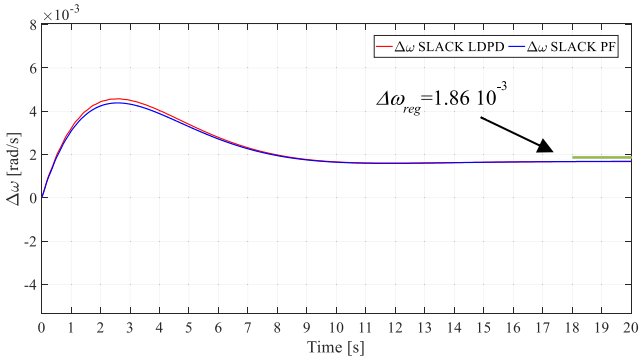

FIGURE 15. Angular frequency deviations of the slack bus after a disturbance with LDPD and with PF for the 29-bus grid.

quency deviation $\Delta\omega_{ref}$ after the transient (green line): it is in accordance with the simulated behaviour. This agreement can be observed also in Fig. 16, where all network generator angular frequencies are shown, by considering the complete generator model in PF.

It is worth noting how the linearized dynamic enhances the oscillatory phenomena (with a less damping effect) with respect to the complete generator model.

In Table 2 the main computed quantities related to the angular frequency behaviours are reported, by comparing LDPD, PF and TH.

From Table 1 and Table 2, it is possible to observe how the deviations of the LDPD with respect to the reference theoretical calculations keep practically unchanged compared to the 17-bus grid. The maximum angular frequency deviations of the LDPD with respect to the PF presents a displacement compared to the 17-bus case study, but always with a difference less than 4%. This displacement is due to the higher complexity of the network, which makes less licit the dynamic linearization.

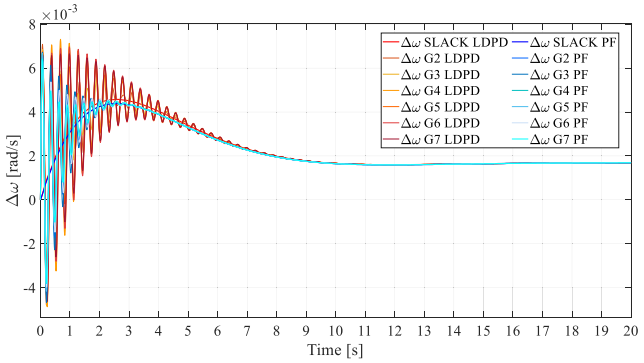

FIGURE 16. Angular frequency deviations of all the generator buses after a disturbance with LDPD and with PF (complete PF generator model) for the 29-bus grid.

TABLE 2. Comparison of absolute values and percentage errors of dynamic response quantities for 29-bus grid.

		Theoretical – One generator plus Loads (TH)	*LDPD*	*PF*
$\Delta\omega_{reg}$	[rad/s]	0.00186	0.00167	0.00169
	%	-9.9 *	/	1.19 **
$\Delta\omega_{max}$	[rad/s]	0.00495	0.00456	0.00438
	%	-9.9 *	/	-3.94 **
$\Delta\omega_{reg}$	[rad/s]	2.643	2.64	2.58
	%	-0.19 *	/	-2.27 **

* Percent difference $\frac{LDPD-TH}{TH}\cdot 100$

** Percent difference $\frac{PF-LDPD}{LDPD}\cdot 100$

In the following, a sensitivity analysis is performed, in order to show how a change in one parameter modifies the angular frequency deviation behaviour and to show if it happens indifferently for LDPD and for PF dynamics.

The first analysis aims at showing what happens with the change in the time regulation constant value T_R for the slack bus generator, from *10* s to *5* s.

Fig. 17 shows how the regulation constant decrease leads to a greater promptness in the regulator response and to a less pronounced overshoot, in accordance with the theory.

In the steady-state regime, the frequency deviation correctly returns to the same value since the frequency droop (and hence the regulating energy) is the same in both cases.

With the second analysis, a slack-bus generator frequency droop decreasing is performed. Fig. 18 shows that in the steady-state regime the frequency deviation goes to a lower value and during the transient regime the frequency overshoot remains less pronounced. This behaviour is justified by the gain increase of the closed-loop transfer function of the control loop.

It is worth noting the effect of such a variation in the eigenvalue diagram of the LDPD state matrix. From Fig. 19, it can be seen that, in the lower droop case, the eigenvalues contributing for the most part to the state variable $\Delta\omega$ of the slack-bus, present a negative real part with a higher

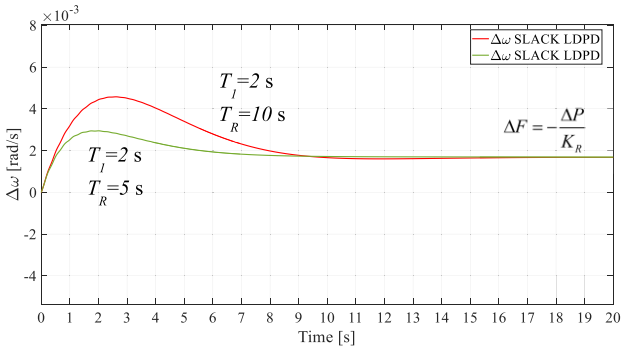

FIGURE 17. Angular frequency deviations of the slack-bus after a disturbance with LDPD for the 29-bus grid with $T_R = 5$ s and $T_R = 10$ s.

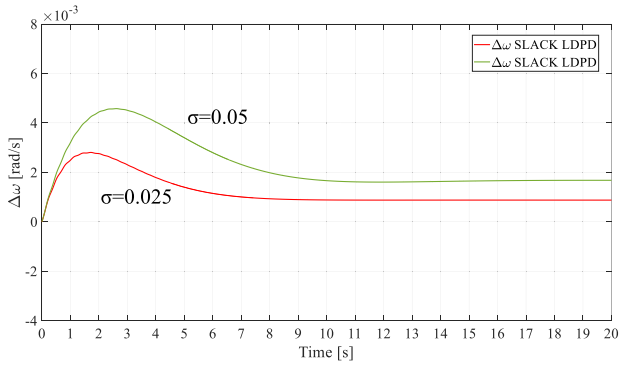

FIGURE 18. Angular frequency deviations of the slack-bus after a disturbance with LDPD for the 29-bus grid with $\sigma = 0.025$ and $\sigma = 0.05$.

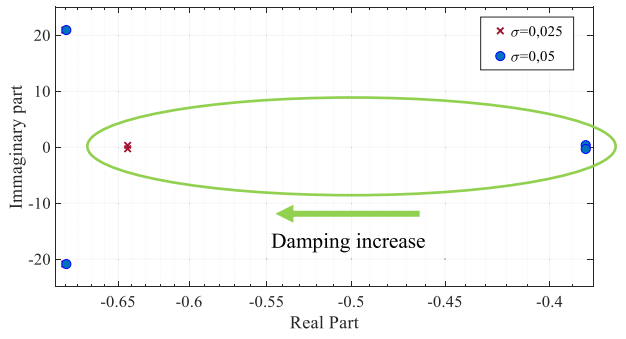

FIGURE 19. Detail of the state matrix eigenvalues diagram of the LDPD for the 29-bus grid with $\sigma = 0.025$ and $\sigma = 0.05$.

magnitude. This means that the corresponding modes have got a higher damping, as shown in the time-domain behaviour of Fig. 18.

LDPD also offers the possibility to study the angular frequency deviation behaviours by varying the portion of asynchronous rotating loads, as both a static and a dynamic variation. Consequently, it is interesting to analyse the frequency behaviour by varying this parameter.

In particular, Fig. 20 and Fig. 21 show how the frequency behaviour changes in accordance with the following load properties, for the generator 1 (see Fig. 20) and for the generator 2 (see Fig. 21) respectively:

1. $Q_s = 1$; $Q_d = 0$ (standard case);

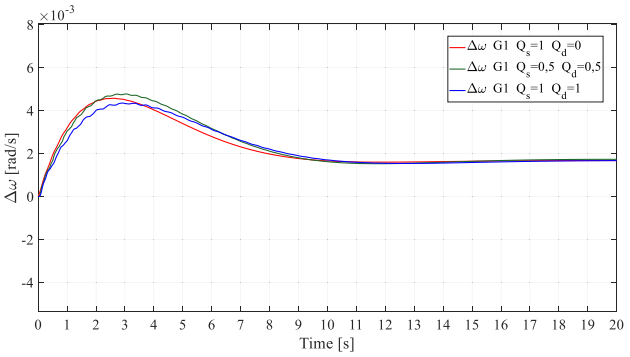

FIGURE 20. Angular frequency deviations of the slack-bus computed with LDPD after a disturbance in the 29-bus grid with different share of asynchronous load.

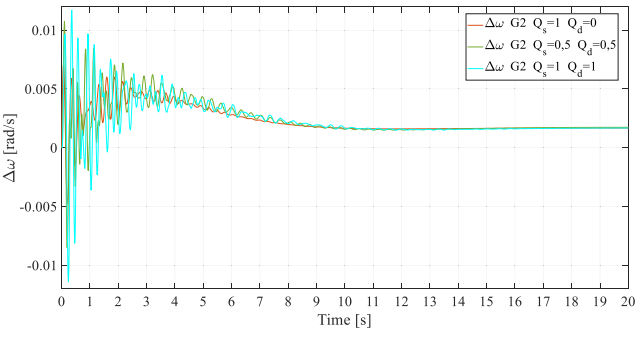

FIGURE 21. Angular frequency deviation of G2 after a disturbance with LDPD for the 29-bus grid with different share of asynchronous load.

2. $Q_s = 0.5$; $Q_d = 0.5$ ($T_{as} = 3$ s);
3. $Q_s = 1$; $Q_d = 1$ ($T_{as} = 3$ s)

where Q_s provides the load share with a static dependence by the frequency and Q_d provides the load share with a dynamic dependence by the frequency, by considering conventionally a starting time for loads equal to 3 s.

From Fig. 20 it can be seen how the increase of the asynchronous load share of the dynamic type makes the frequency derivative at the starting time decrease since the global network starting time increases.

It can be also highlighted how in the case of $Q_s = 0.5$ the frequency overshoot is higher, since load participates less in the frequency regulation, resulting in a less damping frequency.

Fig. 21 shows the influence of the dynamic type asynchronous load share in the frequency deviation behaviour for the generator G2. It is evident that this type of dynamic load enhances the oscillations of the less powerful generators. This phenomenon can also be seen in the eigenvalue diagram of Fig. 22. There is an increase in the imaginary part of the oscillatory modes (related to the oscillation amplitude) by increasing the asynchronous load.

C. SICILY POWER SYSTEM ISLANDED AND INTERCONNECTED OPERATIONS

In this section, the results from the study of the linearized dynamic behaviour applied to the Sicily power system are presented. Two main case studies are analysed: the Sicily grid

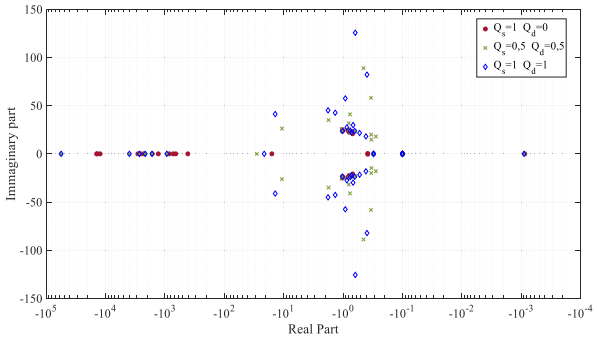

FIGURE 22. Detail of the state matrix eigenvalue diagram of the LDPD for the 29-bus grid with different share of asynchronous load.

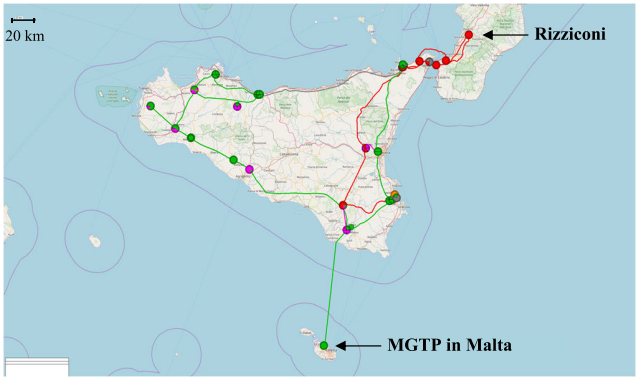

FIGURE 23. Sicily network.

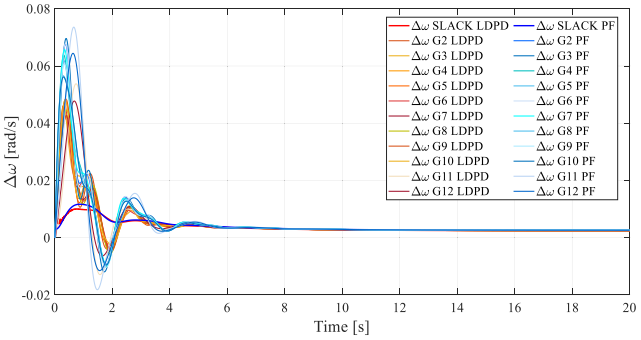

FIGURE 24. Angular frequency deviations of all generators after a disturbance of interconnected Sicily with LDPD and PF.

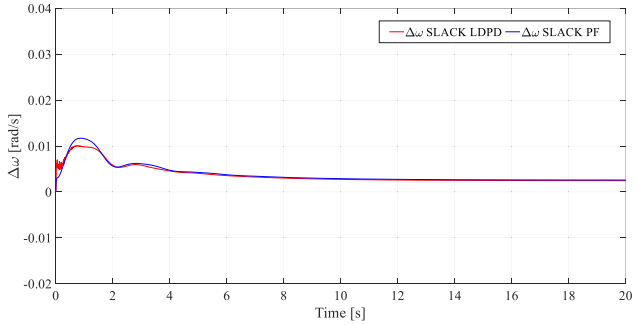

FIGURE 25. Angular frequency deviations of the slack-bus after a disturbance of the interconnected Sicily with LDPD and PF.

connected with the mainland and the Sicily grid in islanding operation.

In the first case, the mainland grid is modelled by an equivalent generator placed in the "Rizziconi" power plant (the red circle in the top-right of Fig. 23).

Fig. 23 shows the substations represented by dots coloured according to these voltage levels:

- Red for 400 kV;
- Green for 220 kV;
- Violet for 150 kV;
- Ochre for 15 kV;
- Grey for out of service.

The first approach is to consider the Sicily grid interconnected with the mainland, i.e. with the pan-European electric power grid. With this aim, it is chosen to attribute a regulating energy of 50000 [MW/Hz] to the equivalent generator placed in "Rizziconi", i.e. the regulating energy value imputable to the European grid in the daytime.

$$K_R = \frac{S_n}{\sigma f_n} \tag{49}$$

From (49) the equivalent droop to be attributed to the slack bus generator can be calculated, (i.e. $\sigma = 0.24 \cdot 10^{-3}$), by considering the generator apparent power $S_n = 600$ MVA.

Let us compute the linearized dynamic behaviour and the complete one of the network after an active power disturbance at the 37-node (MGTP substation).

The disturbance is equal to 15.78 MW (10% of the total absorbed active power of 157.78 MW) which corresponds to 1.4% of the total absorbed power in the Sicily grid in a low-load condition ($P_{Sicily} = 1106.60$ MW). This disturbance can be considered as a "small disturbance" to be studied by a linearized dynamic.

Fig. 24 reports the angular frequency deviation behaviours of all the generators after the disturbance, both for the case study implemented in PF (shades of blues) and in LDPD (shades of red).

In Fig. 25 only the slack generator behaviours are reported. It is worth noting that the behaviour of the slack generator angular frequency deviation is similar for the two cases during the transient and the steady state regime. It can also be observed that the generator angular frequency oscillates around the grid-interconnected frequency, as one would expect in a real situation.

In Fig. 26 the eigenvalue complex space is reported, respectively for LDPD and PF. For the x-axis, a logarithmic scale is applied. The state variables considered for the Modal Analysis in PF are different from those of the present approach. Despite this, by means of an analysis of the participation factors, it is verified that the eigenvalues related to the modes participating for the majority to the generator angular frequency are placed in the central part of the complex plane, around the value of 10^0.

Fig. 26 shows this part of the plane. It confirms the effectiveness of the obtained results also for the calculation of the eigenvalues.

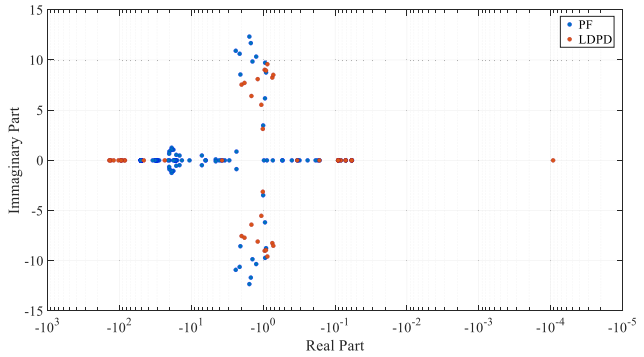

FIGURE 26. Detail of the state matrix eigenvalue diagram of the LDPD and of the PF modal analysis for Sicily interconnected grid.

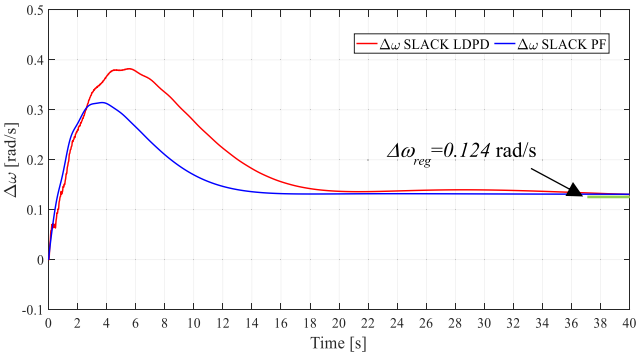

FIGURE 28. Angular frequency deviations of the slack-bus of the islanded Sicily grid after a disturbance with LDPD and PF.

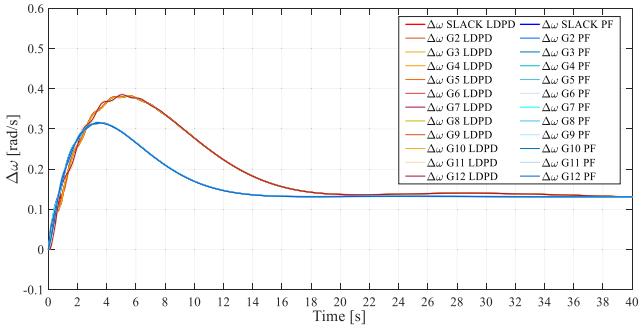

FIGURE 27. Angular frequency deviations of all the generators of the islanded Sicily grid after a disturbance with LDPD and PF.

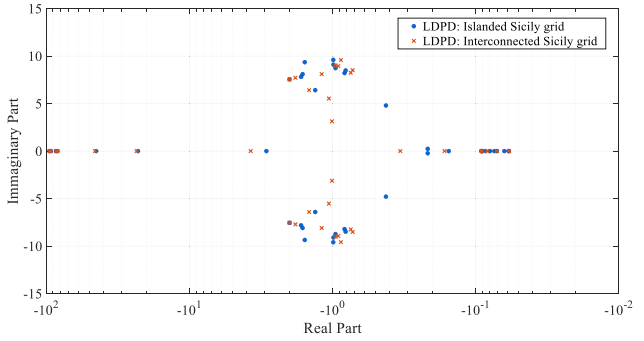

FIGURE 29. Detail of the state matrix eigenvalue diagram of LDPD for Sicily interconnected grid and Sicily islanded grid.

The most interesting result of this part is the static stability of this particular configuration of the grid, which arises both from the angular frequency behaviour and from the eigenvalues analyses.

The second case study regards the Sicily grid in an islanded operation. The active power flowing from the Italian grid is attributed to the slack-bus, whose droop is set to 5 %. In this way, Sicily HV grid is considered without an external interconnection: the generators, with a regulation capability, act in response to a small disturbance.

This particular operating condition, corresponding to a real operating scenario, ensures the power-flow convergence and the static stability of the whole isolated system.

The applied disturbance is the same as before, equal to 15.78 MW (10% of the total absorbed active power of 157.78 MW) which corresponds to 1.4% of the total absorbed power in the Sicily grid in a low-load condition ($P_{Sicily} = 1106.60$ MW).

Fig. 27 shows the angular frequency deviation behaviours of all the generators after the disturbance, both for the case study implemented in PF (shades of blues) and for LDPD (shades of red). In Fig. 28, only the slack bus generator behaviours are reported.

It is worth noting that also in this case the qualitative behaviour of the generators for the two cases is the same. The steady-state value of frequency deviations for the two models are corroborated by TH in (46), indicated by a green line in Fig. 28. The displacement observed in the transient state can be attributed partly to the actual nature of the islanded network: the absence of an extensive grid makes the hypothesis of constant voltage fail at the network nodes during the electromechanical transient, on which LDPD is based.

This hypothesis is well verified when the multi-machine dynamic is performed for a network where the regulating energy of the upstream network prevails over the sum of the regulating energies of the grid generators (as for the reference networks and for Sicily connected to the mainland).

However, the islanded operation for the Sicily grid is not a normal network operation, but it happens only when a failure on the interconnection lines occurs.

From Fig. 29, it can be ascertained how the eigenvalue diagram changes between the interconnected and the islanded Sicily operation. For both cases, the eigenvalues related to angular frequency deviations of generators, in the central part of the diagram, have a smaller imaginary part for the case of interconnected Sicily, respect to the case of islanded Sicily. Such a behaviour confirms the higher damping and the lower magnitude of the generator amplitude in a network with a higher regulating energy compared to a network with a lower regulating energy.

V. CONCLUSION

The paper thoroughly presents a fully implementable algorithm that allows analytically computing both the state and input matrices and also the angular frequency deviations of synchronous generators during an active power

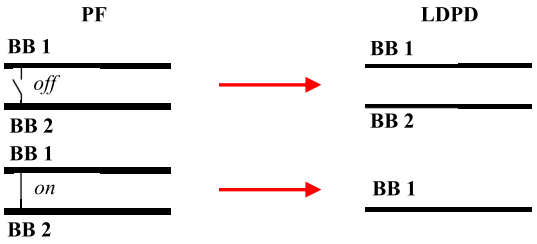

FIGURE 30. Substations bus management.

step disturbance. The students of Electrical Engineering of the University of Padova implement the present procedures in Matlab environment, but other Math-packages can be used. Extensive comparisons between LDPD and PF show a good agreement of frequency deviation behaviours. The compared case studies are reference grids and chiefly the Sicily grid.

Consequently, the present LDPD gives an effective orientation of the multimachine transient stability. The choice of developing fully implementable self-made algorithms is in tune with other researches of Padova **EETL** (**E**lectric **E**nergy **T**ransmission **L**aboratory) [12], [33] and with the didactical approach of Power System Courses at the University of Padova.

APPENDIX
THE INTERFACE PROCEDURE

The interface procedure between PF and LDPD allows passing automatically from a real complex network to an essential network feeding the input data of LDPD. This step is crucial because LDPD needs a strictly ordered topology involving a connected graph where every node can be a PV node, a PQ node or a slack bus.

The procedure uses Microsoft Excel as a bridge between the PF *flexible data* and the Matlab input matrices. In fact, the Matlab matrices contain all topological and typological information about the network. There are essentially two different issues about the topological structure, which the interface procedure has to face with.

The first issue concerns the management of the substation busbars. For example, in order to maintain the correct grid topological consistency, two connected busbars must be considered as a single node in Matlab. This issue is solved as shown in fig. 30. It can be noted that the presence of switches (which are controlled elements existing in real grids: disconnectors and circuit breakers) is suitably treated by the interface program. In fact, if switch is *on* a single node is created, if it is *off* an open circuit is created.

The second issue deals with the presence of more than one edge component insisting on the same node (e.g. one generator and one load insisting on the same bus bar). In this case, a fictitious line is automatically generated as shown in Fig. 31. This figure shows the values of the line length and of r, l, c. They are chosen to simulate a short-circuit connection, but, at the same time, not to create numeric problems in the Matlab-based algorithm (e.g. ill-conditioned network).

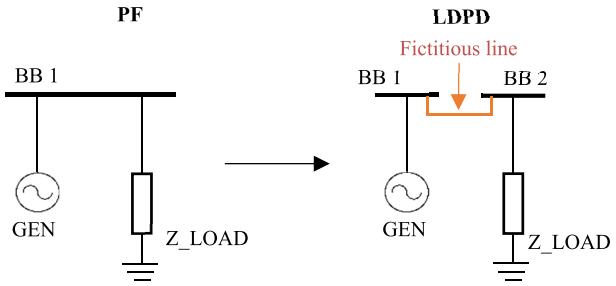

Line length [km]	r [mΩ/km]	l [mH/km]	c [nF/km]
0.01	10	1.2	10

FIGURE 31. Fictitious line management and line parameters.

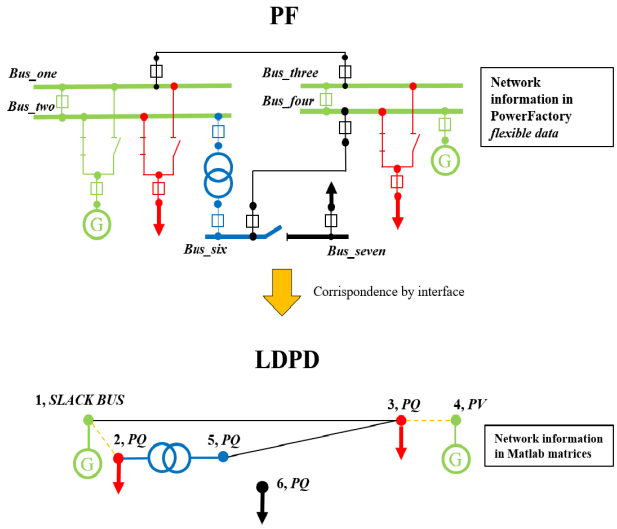

FIGURE 32. Schematic representation of the transfer from a real complex network in PF to an essential network in LDPD (this correspondence is created by exploiting the interface procedure).

The impact of these lines in the power flow and in the dynamic studies is almost null due to their lengths: their influence could be compared to the impact of real substation busbars.

In this way, data about nodes in Matlab environment - pertaining to the new corresponding network - are created.

On the contrary, the information about connections and typologies are treated more simply. In fact, the interface procedure extracts data from *flexible data* PF and creates matrices containing all the parameters modelling the real transmission elements (e.g. *generators*, *3-winding transformer*, *lines*, *shunt*, etc.). The interface procedure is also characterized by the presence of check procedures: they are useful programs to verify if correspondence is achieved in a correct manner, especially for very large transmission networks.

In this way, a univocal correspondence is created and the network can be studied correctly with LDPD. In Fig. 32 the procedure to rebuild a network in Matlab from PF is shown schematically.

ACKNOWLEDGMENT

This article is dedicated to the memory of Professor Antonio Paolucci who always reminded us of the importance of linearized electromechanical dynamics.

From above, Antonio rejoices over his dream coming true: a School of Electric Energy Transmission at the University of Padova.

REFERENCES

[1] R. Benato, N. Crocamo, G. M. Giannuzzi, F. Sanniti, and R. Zaottini, "Multimachine electromechanical response: Comparison between DigSilent and MATLAB-based linearised Behaviour," in *Proc. AEIT Int. Annu. Conf. (AEIT)*, Sep. 2020, pp. 1–6.

[2] J. Machowski, J. W. Bialek, and J. R. Bumby, *Power System Dynamics and Stability*, 3rd ed. Hoboken, NJ, USA: Wiley, 2020.

[3] R. Marconato, *Electric Power Systems*, vol. 2. Pittsburgh, PA, USA: CEI, 2002.

[4] E. W. Kimbark, "Power system stability," in *Synchronous Machines*, vol. 3. Hoboken, NJ, USA: Wiley, 1956.

[5] P. Kundur, *Power System Stability and Control*. New York, NY, USA: McGraw-Hill, 1994.

[6] P. Anderson and A. Fouad, "Power system control and stability," in *IEEE Press Power Engineering Series*. Piscataway, NJ, USA: Wiley, 2003.

[7] P. Kundur, G. J. Rogers, D. Y. Wong, L. Wang, and M. G. Lauby, "A comprehensive computer program package for small signal stability analysis of power systems," *IEEE Trans. Power Syst.*, vol. 5, no. 4, pp. 1076–1083, Nov. 1990.

[8] M. Castrovilli and R. Marconato, "Construction of linearized models of electric power systems for stability studies," *L'Energia Elettrica*, vol. 5, no. 56, pp. 231–238, 1979.

[9] G. C. Verghese, I. J. Péerez-Arriga, and F. C. Schweppe, "Selective modal analysis with application to electric power systems, Part I: Heuristic introduction, Part II: The dynamic stability problem," *IEEE Trans. Power App. Syst.*, vol. PAS-101, no. 9, pp. 3117–3134, Sep. 1982.

[10] A. B. Iskakov and I. B. Yadykin, "Lyapunov modal analysis and participation factors with applications to small-signal stability of power systems," Sep. 2019, *arXiv:1909.02227*. [Online]. Available: https://arxiv.org/abs/1909.02227

[11] I. B. Yadykin, A. B. Iskakov, and A. V. Akhmetzyanov, "Stability analysis of large-scale dynamical systems by sub-gramian approach," *Int. J. Robust Nonlinear Control*, vol. 24, nos. 8–9, pp. 1361–1379, May 2014.

[12] R. Benato, A. Paolucci, and R. Turri, "Power flow solution by a complex admittance matrix method," *Eur. Trans. Electr. Power*, vol. 11, no. 3, pp. 181–188, 2001.

[13] A. A. Bhatti, "Transient and steady state solution of N-dimensional coupled networks and development of equivalent pi and t matrix networks with distributed parameters," in *Proc. 4th Int. Conf. Power Eng., Energy Electr. Drives*, May 2013, pp. 1195–1199.

[14] R. Benato, R. Caldon, A. Mari, and A. Paolucci, "Analytical formation of the state matrix of a regulated power system accounting for UPFC action," in *Proc. UPEC*, Belfast, Northern Ireland, Sep. 2000, p. 186.

[15] R. Benato, R. Caldon, A. Paolucci, and A. Scala, "Analytical procedure for investigating the electromechanical response of a linearised power system with dispersed generation," in *Proc. 37th Universitie Power Eng. Conf. UPEC*, Stafford, U.K.: Staffordshire Univ., 2002, pp. 759–763.

[16] A. Paolucci, *Lezioni di Trasmissione dell'Energia Elettrica*, 4th ed. Padova, Italy: Cleup, 1998.

[17] J. Dou, B. Zhang, and R. Chai, "Electromechanical transient modeling of AC/DC hybrid system incorporating VSC based DC grid," in *Proc. IEEE PES Asia–Pacific Power Energy Eng. Conf. (APPEEC)*, Oct. 2016, pp. 2328–2332.

[18] Y. Susuki, T. Hikihara, and H.-D. Chiang, "Discontinuous dynamics of electric power system with DC transmission: A study on DAE system," *IEEE Trans. Circuits Syst. I, Reg. Papers*, vol. 55, no. 2, pp. 697–707, Mar. 2008.

[19] X. Yang and C. Chen, "HVDC dynamic modelling for small signal analysis," *IEE Proc. Gener., Transmiss. Distrib.*, vol. 151, no. 6, pp. 740–746, Nov. 2004.

[20] M. Zhang and X. Yuan, "Modeling of LCC HVDC system based on mass-damping-spring concept," in *Proc. IEEE Power Energy Soc. Gen. Meeting (PESGM)*, Jul. 2016, pp. 1–5.

[21] L. Zhang, L. Harnefors, and H.-P. Nee, "Modeling and control of VSC-HVDC links connected to island systems," *IEEE Trans. Power Syst.*, vol. 26, no. 2, pp. 783–793, May 2011.

[22] *Partecipazione Alla Regolazione Di Frequenza e Frequenza-Potenza, Allegato 15, Codice di rete italiano*, TERNA SpA, 2008.

[23] I. Report, "Dynamic models for steam and hydro turbines in power system studies," *IEEE Trans. Power App. Syst.*, vols. PAS–92, no. 6, pp. 1904–1915, Nov. 1973.

[24] P. W. Sauer and M. A. Pai, *Power System Dynamics and Stability*. Upper Saddle River, NJ, USA: Prentice-Hall, 1998.

[25] H. Edelmann, *Berechnung Elektrischer Verbundnetze*. Berlin, Germany: Springer, 1963.

[26] O. G. C. Dahl, "Electric power circuits theory and applications," vol. 2. New York, NY, USA: McGraw-Hill, 1938.

[27] K. Ogata, *Modern Control Engineering*, 5th ed. Upper Saddle River, NJ, USA: Prentice-Hall, 2010.

[28] G. Strang, *Differential Equations and Linear Algebra*. Wellesley, MA, USA: Wellesley-Cambridge Press, 2015.

[29] R. C. Dorf and R. H. Bishop, *Modern Control Systems*. London, U.K.: Pearson, 2008.

[30] R. A. DeCarlo, *Linear Systems*. Upper Saddle River, NJ, USA: Prentice-Hall, 1989.

[31] *Technical Reference Documentation for Synchronous Machine*, DigSilent, Berlin, Germany, 2017.

[32] *Guide for Synchronous Generator Modelling Practices and Applications in Power System Stability Analyses*, Standard 1110-2002, 2002.

[33] R. Benato, G. Bruno, S. D. Sessa, G. M. Giannuzzi, L. Ortolano, G. Pedrazzoli, M. Poli, F. Sanniti, and R. Zaottini, "A novel modeling for assessing frequency Behavior during a hydro-to-thermal plant black start restoration test," *IEEE Access*, vol. 7, pp. 47317–47328, 2019.

ROBERTO BENATO (Senior Member, IEEE) was born in Venezia, Italy, in 1970. He received the Dr.-Ing. degree in electrical engineering from the University of Padova, in 1995, and the Ph.D. degree in power systems analysis, in 1999. In 2011, he was appointed as an Associate Professor with the Department of Industrial Engineering, Padova University. He is the author of 190 articles and four books, edited by Springer, Wolters Kluwer, and China Machine Press. He has been a member of six Cigré Working Groups (WGs) and the IEEE PES Substations Committee and a Secretary of two Joint WGs. In 2014, he has been a nominated member of IEC TC 120 "Electrical Energy Storage (EES) Systems" at the WG 4 "Environmental Issues of EES Systems." In 2015, he has been a nominated Member of IEC TC 115 "High Voltage Direct Current (HVDC) transmission for DC voltages above 100 kV" and IEC TC 122 "UHV AC transmission systems." He is also a member of AEIT. In 2017, he has been elected to the grade of a Cigré Distinguished Member.

NUNZIA CROCAMO was born in Salerno, Italy, in 1992. She received the Dr.-Ing. degree in electrical engineering from the University of Naples Federico II, in 2017. Since 2018, she has been with TERNA. She is currently an Engineer with the Dispatching and Switching Department–Stability and Network Calculations and an Expert in static and dynamic studies.

GIOVANNI GARDAN (Member, IEEE) was born in Padova, Italy, in 1995. He received the M.Sc. degree in electrical engineering from the University of Padova, in 2020, with a thesis about the study of power flow solution of Italian electrical grid. Soon after graduating, he joined the Power System Research Group with the Department of Industrial Engineering, Padova University. His main fields of research interests include electrical energy transmission and computer analysis of power systems. He is a Young Member of both Cigrè and AEIT.

GIORGIO M. GIANNUZZI received the degree in electric engineering from the University of Rome. Till December 2000, he worked with ABB, where he was in charge of network studies, protection, and control applications, with special reference to RTU apparatus and data engineering issues. Since 2001, he has been working with TERNA as an Expert in defense plans/systems, dynamic studies, protection, telecontrol, and substation automation. From 2004 to 2011, he coordinated the study, design, and activation of Wide Area Defense system (including interruptible customers system) and a Wide Area Monitoring System. In addition under his guidance, the main security Energy Management Systems were designed and coded, they are actually in use with the National Control Centre (optimal power flow security and market constrained, optimal reactive power flow, dynamic security assessment tool, dynamic and static security verification software, and operator training simulator). He supervised the revision of main Italian Grid Code technical enclosures (primary and secondary frequency regulation, load shedding, protection and automation, and defense plans). Till 2009, he was a member of the UCTE Expert Group on power system stability. In 2010, he joined the ENTSO-E System Protection and Dynamics Group. Starting from 2014, he is the Convener, coordinating the European evaluation over dispersed generation impact on system security and load shedding guidelines. He is currently responsible for the Engineering Department of National Dispatching Centre.

COSIMO PISANI was born in Benevento, Italy, in 1985. He received the M.Sc. degree (Hons.) in energy engineering from the University of Sannio, Benevento, in 2010, and the Ph.D. degree in electrical engineering from the University of Naples Federico II, Naples, Italy, in 2014. During his Ph.D. in collaboration with TERNA, he investigated some dynamic stability issues of large interconnected power system, such as the European one. From May 2014 to March 2016, he was a Research Fellow with the University of Sannio. From March 2016, he is with TERNA. He is currently a Senior Power System Engineer with the Dispatching and Switching Department–Stability and Network Calculations. He is the author or coauthor of over 60 scientific articles. His research interests include applications of dynamic stability of power systems, wide area monitoring and protection systems, high voltage direct current systems, and power system restoration. He is a Leader of WAMS task force within ENTSO-E System Protection and Dynamic. He was a member of the CIGRE C2.17 working group Wide Area Monitoring Systems–Support for Control Room Applications. He is currently a member of the CIGRE C2.18 working group Wide Area Monitoring Protection and Control Systems–Decision Support for System Operators.

FRANCESCO SANNITI (Member, IEEE) was born in Feltre, Italy, in 1994. He received the Dr.-Ing. degree in electrical engineering from the University of Padova, in 2019. He is currently pursuing the Ph.D. degree attending the Postgraduate Course in industrial engineering with the Department of Industrial Engineering, University of Padua. His main fields of research interests include dynamic modeling of frequency-voltage control systems for power system restoration, cables and OHL sequence impedance calculation, extremely high-voltage–high-voltage transmission lines, and advanced materials techniques for static and dynamic power system analysis. He is a Young Member of both CIGRÉ and AEIT.

ROBERTO ZAOTTINI received the degree in electrical engineering from the University of Rome 'La Sapienza', in 1999. In 1997, he worked as a EDP-Consultant in collaboration with Autostrade. In 2000, he worked with telecommunications company, Infotel, in association with Ericsson. Since 2001, he has been working with Italian TSO (TERNA), as an Expert in static and dynamic studies, defense plans/systems, and restoration strategies. He contributed to the implementation of new restoration strategies between different TSO (total path over 1400 km up to a large power plants and use of shunt reactors) through coordination of all relevant actors and electromagnetic and electromechanical simulations. Till 2005, he was a member of the UCTE Expert Group on Power System Stability. From 2010, he is a member of the ENTSO-E System Protection and Dynamics Group (SPD). In 2013, (SPD Expert Group) has been produced an ENTSO-E report ''Dispersed Generation impact on CE Region Security.'' He is a member of the Project Team of Advanced use of HVDC links in system operations. He was the Italian Member of the Cigré Working Group ''System Restoration Procedures and Practices.'' He is also a member of the Cigré Working Group ''Operating Strategies and Preparedness for System Operational Resilience.''